Available online at www.sciencedirect.com
SCIENCE DIRECT®
International Journal of Heat and Mass Transfer 47 (2004) 899–911
International Journal of HEAT and MASS TRANSFER
www.elsevier.com/locate/ijhmt

Mass transfer on and within a frost layer

Byeongchul Na [1], Ralph L. Webb *

Department of Mechanical Engineering, The Pennsylvania State University, 206 Reber Building, University Park, PA 16802, USA

Received 10 May 2003; received in revised form 29 August 2003

Abstract

This paper investigates fundamental phenomena related to understanding of frost deposition and growth. The water vapor mass transfer rate from the air stream to a frost surface was tested and the results analyzed. The water vapor pressure at the frost surface was found to be supersaturated, and this phenomenon is explained using laminar concentration boundary layer analysis. A simple equation for calculating the supersaturated water vapor density at the frost surface was developed using boundary layer analysis, and it was compared to the experimental data. The comparison showed that the proposed equation for the water vapor supersaturation degree at the frost surface agrees well with the experimental data. The physical meaning of the tortuosity factor, which is related to mass diffusion within the frost layer, is mathematically explained, and published correlations were reviewed. It was found that some existing correlations are basically empirical curve fits that force agreement of the frost growth rate with the measured values. Further, these empirical curve fits do not satisfy the known physical bounds on the tortuosity factor. This deficiency further supports the existence of supersaturation at the frost surface. The effect of uncertainty in tortuosity factor on the heat transfer rate through a frost layer was quantitatively analyzed, and it was found that its uncertainty does not significantly affect the heat transfer rate through the frost layer in typical frosting conditions.

1. Introduction

Frost formation on a cold surface occurs by the mass transfer of the water vapor from the air to the cold surface or the frost surface. Some of the water vapor transferred from the air flow to the frost layer deposits on the frost surface, making the frost layer thicker. The rest of the water vapor moves into the frost layer by molecular diffusion, resulting in the frost layer becoming more dense. Thus, precise estimation of the mass transfer rate is very important to predict the frost growth rate and densification rate of the frost layer.

Previous researchers have used the heat and mass transfer analogy to obtain the mass transfer coefficient at the frost surface. This is reasonable because the dimensionless governing equations for energy and concentration are identical. To calculate the mass transfer rate, the driving potential, which is the water vapor density difference between the air stream and the frost surface, must be established. This requires specification of the water vapor density at the frost surface.

Barron and Han [1] and Brian et al. [2,3] assumed that the water vapor is saturated on and within the frost layer. They determined the water vapor saturation pressure using the saturation curve for water vapor over ice. This assumption was also used by many other researchers, such as Sanders [4], Jones and Parker [5], Sami and Duong [6], Le Gall and Grillot [7], Tokura et al. [8], Lee et al. [9], Tao et al. [10], and Schneider [11]. Mao et al. [12] developed an empirical correlation for the mass transfer coefficient during frost growth. However, this correlation is based on the cold surface temperature (not on the frost surface temperature). It is noted that the exponents on the Reynolds number in the heat transfer and mass transfer correlations are not the same. This means that the heat and mass transfer analogy is not used in their correlation. As noted above,

* Corresponding author. Tel.: +1-814-865-0283; fax: +1-814-865-1344.
E-mail addresses: bxn6@psu.edu (B. Na), r5w@psu.edu (R.L. Webb).
[1] Tel.: +1-814-865-9719; fax: +1-814-865-1344.

0017-9310/$ - see front matter © 2003 Elsevier Ltd. All rights reserved.
doi:10.1016/j.ijheatmasstransfer.2003.08.023

Nomenclature

A	area [m^2]
A_c	cross sectional area normal to the diffusion path [m^2]
c_{pa}	specific heat of air [kJ/kg K]
D_v	water vapor diffusion coefficient [m/s]
D_{eff}	effective water vapor diffusion coefficient in the frost layer defined in Eq. (23) [m/s]
g	function defined in Eqs. (30a) and (30b)
i_{sv}	sublimation energy of water [kJ/kg]
k	thermal conductivity [W/m K]
K_w	mass transfer coefficient based on humidity ratio difference [kg/m^2 s]
LHR	ratio of the latent heat transfer to the total heat transfer
m_a	air flow rate [kg/s]
m_v	water vapor mass transfer rate [kg/s]
m''_v	water vapor mass flux [kg/m^2 s]
m_{vd}	water vapor mass transfer rate by molecular diffusion rate [kg/s]
m''_{vd}	water vapor mass flux by molecular diffusion rate [kg/m^2 s]
Pr	Prandtl number
P_v	vapor pressure [kPa]
P_{vs}	saturated vapor pressure [kPa]
q	heat transfer rate [W]
q''	heat flux [W/m^2]
r	water droplet radius [m]
S	supersaturation degree, $(P_v - P_{vs})/P_{vs}$, as defined by Eq. (1) [–]
s	coordinate following diffusion path [m]
Sc	Schmidt number
St	heat transfer Stanton number
St_m	mass transfer Stanton number
T	temperature [°C]
T_K	temperature [K]
t	Time [s]
u	x-component of air velocity [m/s]
u_∞	free-stream air velocity [m/s]
v	crystal growth velocity [m/s]
W	humidity ratio
ΔW_{lm}	log mean humidity ratio difference defined by $(W_{a,i} - W_{a,o})/\ln((W_{a,i} - W_{fs})/(W_{a,o} - W_{fs}))$
x	coordinate along the flow direction [m]
x_{fs}	frost layer thickness [m]
y	coordinate normal to the flow direction [m]

Greek symbols

ε	porosity
η	similarity parameter, $\eta \equiv y/\sqrt{vx/u_\infty}$
ρ_v	vapor density [kg/m^3]
σ	surface tension of liquid water [N/m]
τ	non-dimensional temperature, $\tau = (T - T_{fs})/(T_\infty - T_{fs})$
τ	tortuosity factor defined in Eq. (26)
ξ_v	non-dimensional water vapor concentration, $\xi_v = (\rho_v - \rho_{v,fs})/(\rho_{v,\infty} - \rho_{v,fs})$
ζ	non-dimensional velocity, $\zeta' = u/u_\infty$

Subscripts

a	air
cr	critical value
exp	experimental value
fr	frost layer
fs	frost surface
i	inlet
ice	ice
lat	latent heat
o	outlet
pre	predicted value
sat	saturation state
sen	sensible heat
v	vapor
w	cold surface
∞	free stream

Miscellaneous

$\bar{}$ (over-bar) mean value in the frost layer

all researchers of the frost formation have assumed that the water vapor is saturated at the frost surface.

Contrary to the previously referenced work, Na and Webb [13] have shown that the water vapor is supersaturated at the solid-vapor interface. The term "supersaturation degree" is defined [4] as

$$S \equiv (P_v - P_{vs})/P_{vs}, \quad (1)$$

where P_v and P_{vs} are the actual local vapor pressure, and the local saturation vapor pressure, respectively. Supersaturation implies that the saturation vapor pressure is less than the local vapor pressure, which means that the vapor is sub-cooled below its saturated state. The $S = 0$ if $P_{vs} = P_v$ and increases as the local vapor subcooling increases.

The concept of supersaturation, as related to condensation of water vapor in air, is well known and is accepted in the fields of thermodynamics, chemistry, and meteorology. For example, when steam is expanded through a turbine nozzle, the water vapor condenses at a temperature below that of saturation [14]. This phenomenon is known as the "Wilson line". Similarly water vapor must be supersaturated for fog to form [15]. Supersaturation is required in these two examples, because the condensed vapor forms very small droplets. Due to surface tension, the vapor pressure surrounding the

Table 1
Heterogeneous nucleation temperature for ice formation in fog [16]

Substances	Nucleation temperature (°C)
Silver iodide	−2.5
Lake Albany clay	−11
Volcanic ash (Crater Lake)	−16
Cryolite	−20
Topaz	−23

droplet is less than that inside the droplet by the amount $2\sigma/r$, where r is the droplet radius. The pressure inside the droplet is very slightly higher than the equilibrium saturation pressure [15]. Hence, the vapor at the liquid–vapor interface is supersaturated. The same conditions occur in ice crystal formation. For example, Fletcher [16] reviewed the published experimental data for ice crystal formation in a supercooled fog and summarized the nucleation temperature for nucleation on various substrates. Table 1 shows their summarized data.

The data shown in Table 1 implies that the water vapor is supersaturated, even if nuclei are supplied to the foggy region to assist ice crystal to form. Na [17] and Na and Webb [13] show that the required supersaturation degree is strongly dependent on the surface energy, which is influenced by coatings that provide different contact angles.

The supersaturation degree at the frost surface is very important for the mass transfer during frost growth because it determines the driving potential for the mass transfer. In this paper, the existence of the supersaturation degree at the frost surface is experimentally validated. Further, analytic formulation for supersaturation degree at the frost surface will be derived and compared to the authors' experimental data. This work thus provides new understanding of mass transfer phenomena in frost deposition and growth.

The tortuosity factor in the frost layer is a key factor in calculating the water vapor molecular diffusion in the frost layer. Many correlations for the tortuosity factor in porous media have been published. However, the correlations were developed empirically and show significant differences one another. Based on the physical meaning of the tortuosity factor, its possible range will be mathematically derived, and range of the tortuosity factor predicted by the existing correlations will be compared to the physical bounds as one means of establishing their validity (or invalidity). Further, the uncertainty in the correlations on the heat transfer through the frost layer and densification of the frost layer will be analyzed for typical frost conditions.

2. Supersaturation at the frost surface

The ice crystal growth rate is dependent on the water vapor supersaturation degree at the ice crystal–water vapor interface. This is because the assimilation of water vapor molecules into the ice crystals requires the chemical potential difference between water vapor and ice crystals at the interface. Based on the chemical potential difference, Fletcher [16] derived the ice crystal growth velocity (v) given by

$$v = K \exp[-A/\ln(P_v/P_{vs})], \tag{2}$$

where K and A are constants, and the ratio $P_v/P_{vs} = (1 + S)$. Eq. (2) shows that it is necessary that the water vapor be supersaturated for ice crystals to grow. Without supersaturation at the frost surface, frost layer cannot grow. However, it is not practical to measure the local vapor pressure at a frost surface, which is required to calculate S. This is likely the reason the prior referenced researchers of frost deposition on a cold surface have generally assumed that the water vapor is saturated at the frost surface. A key purpose of this paper is to define methodology to define the supersaturation degree at the frost surface. At the following section, the approach to obtain the supersaturation degree will be tried.

2.1. Boundary layer analysis

Using boundary layer approximations for laminar flow over a flat plate and the similarity parameter (η) and non-dimensional variables (ζ, τ, and ξ_v) defined in Table 2, the governing equations for momentum, energy, and concentration may be simplified to ordinary differential equations as shown in Table 2. These ordinary differential equations may be solved numerically, and the solutions allow prediction of the local velocity, temperature, and concentration.

Table 2
Non-dimensional boundary layer equations

Boundary layer	Equations	Definitions	Boundary conditions
Momentum	$\zeta''' + \frac{1}{2}\zeta\zeta'' = 0$	$\zeta'(\eta) = \dfrac{u}{u_\infty}$, $\eta = y/\sqrt{vx/u_\infty}$	$\zeta(0) = 0$, $\zeta'(0) = 0$, $\zeta'(\infty) = 1$
Energy	$\tau'' + \frac{Pr}{2}\zeta\tau' = 0$	$\tau = (T - T_{fs})/(T_\infty - T_{fs})$	$\tau(0) = 0$, $\tau(\infty) = 1$
Concentration	$\xi_v'' + \frac{Sc}{2}\zeta\xi_v' = 0$	$\xi_v = (\rho_v - \rho_{v,fs})/(\rho_{v,\infty} - \rho_{v,fs})$	$\xi_v(0) = 0$, $\xi_v(\infty) = 1$

With the calculated local temperature and concentration, the supersaturation degree of water vapor in air stream is obtained. The concentration equation uses as the dependent variable the non-dimensional concentration (ξ_v). The concentration at the frost surface ($\rho_{v,fs}$) is needed to calculate the ρ_v in the boundary layer. Fig. 1 shows the solution for the S vs. η based on two different assumed boundary conditions at the cold surface. Fig. 1a assumes the air is saturated at the cold surface ($S = 0$). Fig. 1b assumes supersaturated air at the cold surface. Attention is first directed at Fig. 1a which shows variation of supersaturation degree (S) in the boundary layer for 50%, 70%, and 100% relative humidity conditions in the air stream. For the higher humidities (70% and 100%), Fig. 1a shows that a maximum supersaturation exists within the boundary layer, rather than at the cold surface. We will prove that this condition is physically impossible. Thus, we will prove that

- a maximum supersaturation cannot occur in the air stream close to the cold surface,
- an inflection point for S cannot occur in the boundary layer.

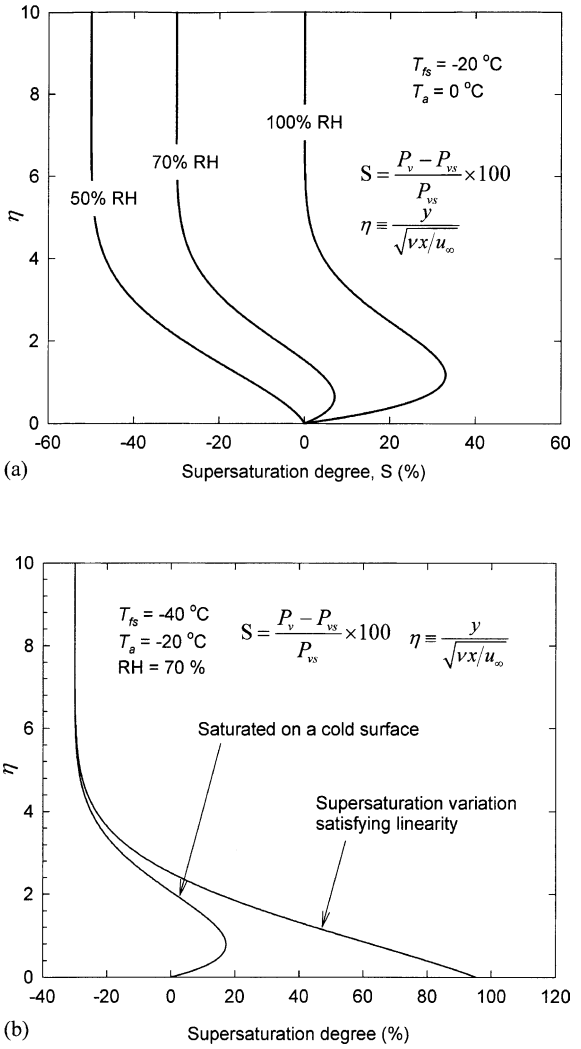

Fig. 1. Supersaturation degree variation in the boundary layer: (a) saturation model; (b) supersaturation model.

Finally, an appropriate procedure to determine and obtain the supersaturation degree at the cold surface will be presented as is illustrated in Fig. 1b.

If the convection term is negligible, the temperature and concentration will vary linearly in the region adjacent to the wall; for example with laminar flow, in the region $\eta < 2$, it can be assumed without significant error that the velocity, temperature, and concentration gradients are linear. Thus the concentration gradient must be a constant for a given mass transfer rate:

$$d\rho_v/dy = \text{constant}. \tag{3}$$

Using the ideal gas relation and definition of the supersaturation degree, Eq. (3) may be written as

$$\frac{d}{dy}\left(\frac{P_v}{T_K}\right) = \frac{d}{dy}\left[\frac{(1+S)P_{vs}}{T_K}\right] = \text{constant}. \tag{4}$$

It is reasonable to assume that the saturation pressure of water varies linearly with saturation temperature in the range of 0 to −40 °C. Thus, we may write

$$\frac{P_{vs}}{T_K} = aT_K + b, \tag{5}$$

where a and b are constants. Using Eq. (5), Eq. (4) may be expressed as

$$\frac{d}{dy}[(1+S)(aT_K + b)] = C. \tag{6}$$

The dimensionless air temperature (τ) varies linearly with η in the region of interest and may be written as

$$\tau = c^*\eta \quad \text{or} \quad T_K = cy + d, \tag{7}$$

where $c = c^*/\sqrt{vx/u_\infty}$ and $d = T_{fs}$. Using Eq. (7), Eq. (6) becomes

$$\frac{d}{dy}[(1+S)(Ay + B)] = C, \tag{8}$$

where $A = ac$ and $B = ad + b$. Integrating Eq. (8) yields

$$S = \frac{C}{A} - \frac{1}{AE(Ay+B)} - 1, \tag{9}$$

where E is a constant resulting that occurs from the integration. Differentiating Eq. (9) with respect to y, gives

$$\frac{dS}{dy} = \frac{1}{E}\frac{1}{(Ay+B)^2}. \tag{10}$$

Eq. (10) shows that the first derivative of S cannot be zero within the region of interest ($\eta < 2$). Therefore, it is a mathematical impossibility to have a supersaturation profile that has a maximum between the air stream and the surface. Taking the second derivative of S yields

$$\frac{d^2S}{dy^2} = -\frac{2A}{E}\frac{1}{(Ay+B)^3}. \tag{11}$$

Inspection of Eq. (11) shows that the second derivative of S cannot be zero within the region of interest ($\eta < 2$). This means that it is mathematically impossible to have an inflection point in the region ($\eta < 2$). Therefore, it is concluded that the supersaturation degree cannot have a maximum point or an inflection between the air stream and the cold surface. The key implication of this is that the air cannot be saturated at the frost surface. Hence, the S vs. η profiles shown on Fig. 1 are invalid.

It is necessary to establish a procedure to obtain the supersaturation degree at the cold surface. Table 3 shows the order of terms Ay and B in Eq. (10) in the near wall region ($\eta < 2$). The order of Ay is much less than that of B. Hence, the gradient of supersaturation degree in the region close to the cold surface may be treated as a constant without significant error. Using the linearity of the supersaturation degree in the near wall region the following procedure is used to obtain S at $\eta = 0$:

(1) Assume S at $\eta = 0$ and calculate the concentration distribution.
(2) The supersaturation degree in the region $\eta < 2$ is obtained from the concentration distribution and temperature distribution in the boundary layer.
(3) Using a linear regression method, the linearity is checked in this region.

This procedure is performed for different values of S at $\eta = 0$. The value of S at $\eta = 0$ is established by the best linear curve of S vs. η. Using the above procedure, Fig. 1b shows an example calculation of the supersaturation degree distribution in the boundary layer and the supersaturation degree at the frost surface. Although this is a straightforward procedure, it requires iteration. A simpler procedure that does not require iteration is given in the next section.

2.2. Simple equation for supersaturation degree at the frost surface

Using the above procedure, we calculated curves of S vs. η for different values of surface temperature, air temperature, and humidity. The curves of S vs. η satisfied the linear condition in the region $\eta < 2$. Next, the values of S at $\eta = 0$ were correlated by the following empirical equation:

$$S_{fs} = 0.808(P_{v,\infty}/P_{vs,\infty})(P_{vs,fs}/P_{vs,\infty})^{-0.657} - 1 \tag{12}$$

$T_{fs} + 14\ ^\circ\text{C} < T_\infty < T_{fs} + 20\ ^\circ\text{C}$,
and $-40\ ^\circ\text{C} < T_{fs} < 0\ ^\circ\text{C}$.

2.3. Experiment for mass transfer rate

Experiments were conducted to validate the procedure used to obtain the supersaturation degree at the frost surface described above. The test surface was fabricated of pure aluminum as shown in Fig. 2. This design is composed of six aluminum fins on the aluminum base to increase the heat transfer area. The heat transfer with air occurs only on the fins. This test surface was located on the cold block shown in Fig. 2. The carbon steel block is cooled by the thermoelectric modules driven by a DC power supply. The heat on the hot side of the thermoelectric modules is removed by the coolant flowing through the heat sink. The temperature of the cold block is controlled by the temperature of the coolant.

The total heat transfer rate from the air to the test section was measured in the carbon steel block in Fig. 2. Four thermocouples were inserted in the carbon steel block, toward the center of the block with 18 mm spacing. The temperature gradient in the block was measured by the thermocouples. Using this temperature gradient, the total heat transfer rate was calculated:

$$q_{total} = -k_{block}A_c(dT_{block}/dx). \tag{13}$$

Table 3
Orders of magnitude in Eq. (10)

Ay									$B = ad + b$		
$A = ac$					$y = \eta\sqrt{vx/u_\infty}$				a	d	b
a	$c = c^*/\sqrt{vx/u_\infty}$										
10^{-1}	c^*	v	x	u_∞	η	v	x	u_∞	10^{-1}	10^2	10^1
	10^0	10^{-5}	10^{-3}	10^0	10^0	10^{-5}	10^{-3}	10^0			
		10^{-1}				10^{-1}				10^1	
		10^{-2}									
				10^{-3}							

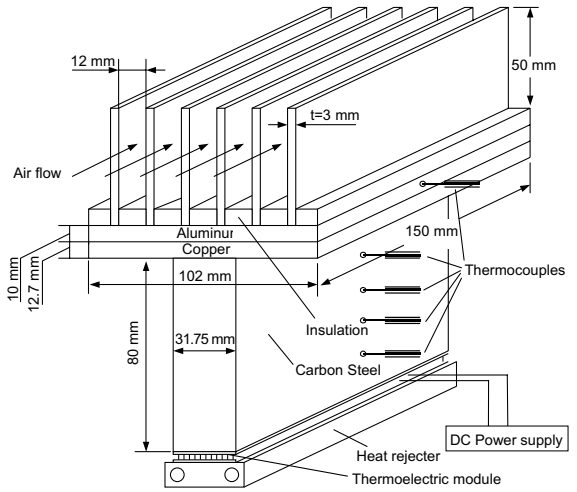

Fig. 2. Test section.

Using the measured air flow rate and air temperature change between the wind tunnel inlet and outlet, the sensible heat transfer rate in the test section was obtained by the following energy balance:

$$q_{\text{sen}} = m_{\text{a}} c_{p\text{a}} (T_{\text{a,i}} - T_{\text{a,o}}), \tag{14}$$

where $T_{\text{a,i}}$ is the air temperature measured at the inlet of the test section, and $T_{\text{a,o}}$ is the test section outlet temperature. While frost deposits on the test surface, latent heat transfer due to the phase change occurs. The latent heat as well as the sensible heat is transferred through the cold block (Fig. 2). Therefore, the latent heat transfer rate can be calculated using the total heat transfer rate through the cold block and the sensible heat transfer rate measured by the air temperature difference. The latent heat transfer rate was calculated as

$$q_{\text{lat}} = q_{\text{total}} - q_{\text{sen}}. \tag{15a}$$

Using this latent heat, the mass transfer rate was calculated by

$$m_{\text{v}} = q_{\text{lat}} / i_{\text{sv}}. \tag{15b}$$

The heat balance was evaluated for the condition of only sensible heat transfer to validate the test facility. The heat transfer rate determined by Eq. (13) agreed with that determined by Eq. (14) within 4%.

2.4. Results and discussion

The mass transfer rate may be predicted using the following equation:

$$m''_{\text{v,pre}} = K_{\text{w}} \Delta W_{\text{lm}}, \tag{16}$$

where ΔW_{lm} is the logarithmic mean driving potential based on the humidity ratio. The driving humidity difference is based on that in the air stream (W_{a}) and at the frost surface (W_{fs}). The humidity ratio at the frost surface was assumed saturated at the frost surface temperature in the prediction shown in Fig. 3a. The mass transfer coefficient in Eq. (16) was calculated using the heat and mass transfer analogy:

$$StPr^{2/3} = St_{\text{m}} Sc^{2/3}. \tag{17}$$

The predicted mass flux is compared to the experimental values measured in this work. During data acquisition, raw data points were taken every 13 s, and each data point was averaged for 300 s after a thin frost layer covered the cold surface. The predicted m''_{v} values were based on two different bases for the humidity ratio at the frost surface (W_{fs}). Fig. 3a shows the ratio of the predicted-to-experimental m''_{v} assuming the air is saturated at the frost surface, which is the assumption of the referenced previous researchers.

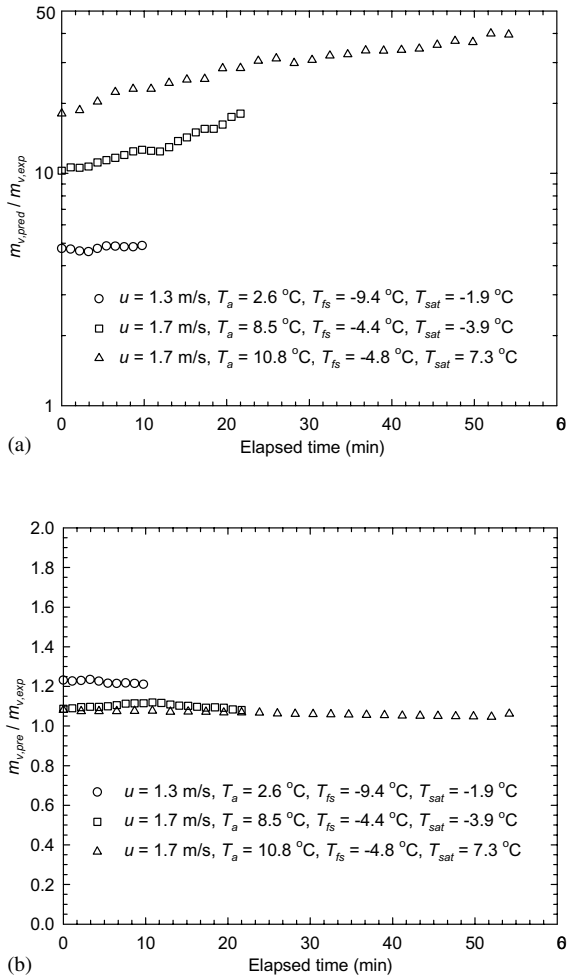

Fig. 3. Comparison of experimental data to predicted data: (a) saturation model; (b) supersaturation model.

As previously noted, all previously published frost growth models assume that the water vapor at the frost surface is saturated at the frost surface temperature. This section evaluates the validity of this assumption. Fig. 3a compares the present experimental data for the mass transfer rate of the water vapor onto the frost surface ($m''_{v,exp}$) to the predicted value ($m''_{v,pre}$) based on the assumption that the water vapor at the frost surface is saturated at the frost surface temperature (saturation model). Fig. 3a shows that the predicted mass transfer rate is 4–30 times the experimental values. However, this does not imply that the frost growth rate is overpredicted by 4–30 times. This is because the frost surface temperature increases as the frost thickness increases. This significantly reduces the frost growth rate. More discussion on this is provided in Na and Webb [18]. Fig. 3b shows the predicted-to-experimental m''_v assuming the air is supersaturated at the frost surface. Because of the supersaturation at the frost surface, the W_{fs} should not be evaluated as $W_{fs,sat}$. Rather, one should calculate $W_{fs} = (1 + S)W_{fs,sat}$ and substitute this in Eq. (16). The S was calculated using Eq. (12) described in Section 2.2. The predicted values are 0–25% higher than the experimental results. Comparison of Fig. 3a and b shows that use of supersaturated conditions at the frost surface results in much more accurate prediction of the mass transfer rate than is yielded by assumption of saturated air at the frost surface. Hence, we conclude that the assumption of saturation at the frost surface is clearly incorrect.

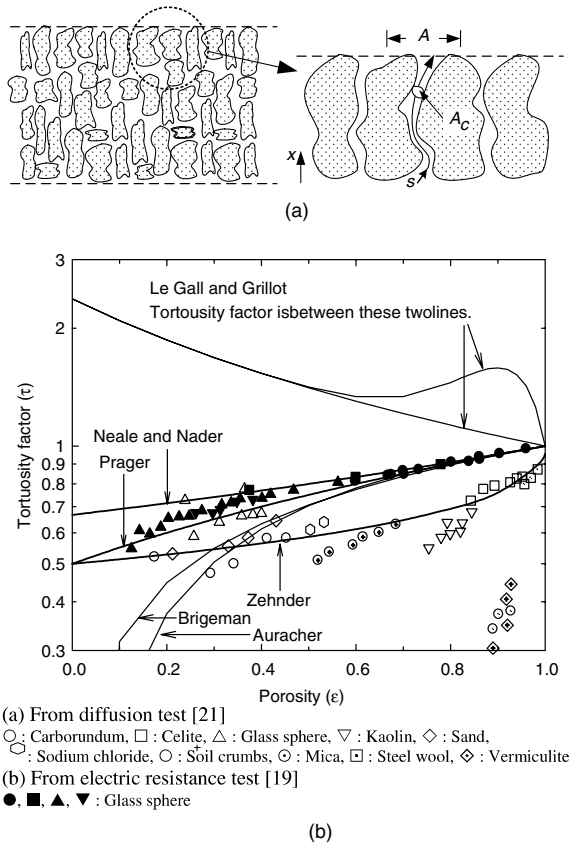

Fig. 4. Mass diffusion in porous media: (a) tortuous diffusion path; (b) comparison of correlations for tortuosity to experimental data.

3. Mass diffusion within the frost layer

Previously published models for the frost growth that assume saturated air at the frost surface have shown first order ability to predict the frost growth rate. The predictions for the frost growth rate are also influenced by the equations used for the tortuosity factor. Thus, the mass transfer rate overpredictions shown in Fig. 3a can be compensated for by overpredictions in the densification of the frost layer, resulting from tortuosity factors empirically chosen to yield acceptable prediction of the frost growth rate. In this section, the physical limit of the tortuosity factor and its effect on the frost layer mechanism will be discussed.

The mass transfer rate within the frost layer is given by multiplying the mass flux by the area normal to the diffusion direction:

$$m_v = -D_v A(\partial\rho_v/\partial x). \tag{18}$$

The coordinate x is shown in Fig. 4a. Diffusion occurs in porous media through the pore regions, and the area in Eq. (18) must be the cross sectional area of the pore region (A_c). Fig. 4a shows the cross sectional area (A_c) in the pore region. The length of the path, along which the diffusion occurs, is greater than that of the porous frost layer thickness, because the pore region is generally tortuous in the porous media. The diffusion mass transfer rate through the pores may be expressed as

$$m_v = -D_v A_c(\partial\rho_v/\partial s), \tag{19a}$$

$$m_v = -D_v A_c(\mathrm{d}x/\mathrm{d}s)(\partial\rho_v/\partial x). \tag{19b}$$

The symbol, s is the length following the diffusion path shown in Fig. 4a. Based on the projected base surface area, A, the mass flux may be expressed as

$$m''_v = \dot{m}/A = -D_v(A_c/A)(\mathrm{d}x/\mathrm{d}s)(\partial\rho_v/\partial x). \tag{20}$$

The local porosity of the porous media is the ratio of the pore volume-to-total volume:

$$\varepsilon_{fr} = (A_c/A)(\mathrm{d}s/\mathrm{d}x). \tag{21}$$

With Eq. (21) for the porosity, the mass flux has the form of

$$m''_v = -D_v\varepsilon_{fr}(\mathrm{d}x/\mathrm{d}s)^2(\partial\rho_v/\partial x). \tag{22}$$

Introducing the effective diffusion coefficient for the porous media defined as

$$D_{\text{eff}} = D_{\text{v}}\varepsilon_{\text{fr}}(\mathrm{d}x/\mathrm{d}s)^2. \tag{23}$$

The mass flux may be expressed as

$$m''_{\text{v}} = -D_{\text{eff}}(\partial\rho_{\text{v}}/\partial x) = -D_{\text{v}}\varepsilon_{\text{fr}}(\mathrm{d}x/\mathrm{d}s)^2(\partial\rho_{\text{v}}/\partial x). \tag{24}$$

In the definition of the effective diffusion coefficient (Eq. (23)), the porosity represents the reduced cross sectional area, and the square of the path length ratio represents the tortuous path of the diffusion.

Some authors have defined the tortuosity factor as $(\mathrm{d}x/\mathrm{d}s)$. However, using the $(\mathrm{d}x/\mathrm{d}s)^2$ definition, which is incorporated into the definition of D_{eff} (Eq. (24)) yields a simple equation for the mass transfer rate. Or, using $\tau = (\mathrm{d}x/\mathrm{d}s)^2$ one may write Eq. (24) as

$$m''_{\text{v}} = -D_{\text{v}}\varepsilon_{\text{fr}}\tau\partial\rho_{\text{v}}/\partial x, \tag{25}$$

$$\tau \equiv (\mathrm{d}x/\mathrm{d}s)^2 = (1/\varepsilon_{\text{fr}})(D_{\text{eff}}/D_{\text{v}}). \tag{26}$$

The tortuosity definition of Eq. (26) is used in this study. Note that Eq. (26) shows that the tortuosity factor cannot be greater than one, because the increment $\mathrm{d}s \geqslant \mathrm{d}x$.

The mass transfer rate is dependent on both the cross sectional area of the diffusion path and the increased path length in porous media. The cross sectional area can be represented by the porosity of the porous media. The diffusion path length will be strongly affected by the shape and packing of the particles constituting the porous media.

Table 4 lists equations that have been proposed for the tortuosity factor for various particle shapes. Fig. 4b shows measured tortuosity values for various particle shapes. The closed symbols were taken by the electric resistance method, and the open symbols by the concentration gradient measurement. Auracher [7] is the only researcher to measure the tortuosity factor of a frost layer. His equation in Table 4 is a curve fit of his experimental data. The porosity of frost is in the range of 0.6–0.9. Examination of Fig. 4b shows that the Auracher correlation agrees quite well with the data for spheres within the porosity range of 0.6–0.9. Further, the correlations of Neale and Nader [19] and Prager [20] agree well with the sphere data in the porosity range of 0.6–0.9. Examination of Fig. 4b shows that τ is strongly dependent on the particle shape. The Zehnder equation was developed to approximately fit the tortuosity factor data for the several shapes on Fig. 4b. However, the Zehnder equation shows poor agreement with the sphere and frost data. Hence, for 0.6–0.9, one may use any of the following equations to reasonably predict the tortuosity factor of frost: Auracher [7], Neale and Nader [19], Prager [20], and Bridgemen [20].

Le Gall and Grillot [7] developed a numerical model for the frost growth rate. They investigated the mass diffusion rate within the frost layer by comparing their numerical model to their experimental data for the frost growth rate. They adjusted the predicted mass diffusion rate by changing the tortuosity factor to force the predicted frost growth to agree to the experimental data. Their tortuosity factor is also shown in Fig. 4b. Their tortuosity factor shows values greater than 1.0, which is not physically possible. Tao et al. [10] also give a tortuosity factor much greater than Le Gall and Grillot. They obtained this by numerical modeling, using an approach similar to that of Le Gall and Grillot. As previously noted, both models assumed saturated vapor at the interface. We do feel that these tortuosity equations are not valid, because the tortuosity factor cannot be greater than one, as noted above. A detailed discussion of the shortcomings of the Le Gall and Grillot and Tao et al. tortuosity factors are given in Na and Webb [16,18].

The above discussion shows that precise predictive equations of the tortuosity factor for a frost layer do not exist. Hence, an important question to evaluate is "How sensitive is the heat transfer rate, densification, and growth rate to the tortuosity factor?" In Section 3.1, this question is analyzed for the limiting cases. The resulting analysis for limiting cases will indicate how much an error in prediction of the tortuosity factor will cause

Table 4
Tortuosity factor correlations

Author	Tortuosity factor	Comments
Brian et al. [3]	$0.769 \leqslant \tau \leqslant 0.909$	Fixed bed of glass particles
Auracher [7]	$\tau = \frac{1}{\varepsilon_{\text{fr}}}\frac{1-\varepsilon_{\text{fr}}}{0.58(1-\varepsilon_{\text{fr}})}$	Frost in capillary tube
Le Gall and Grillot [7]	$\tau = \frac{1}{1-0.58(1-\varepsilon_{\text{fr}})} + F_{\mu}10(1-\varepsilon_{\text{fr}})\varepsilon^{10}$	Numerical adjustment F_{μ} depends on frosting conditions.
Zehnder [4]	$\tau = \left(1-\sqrt{1-\varepsilon_{\text{fr}}}\right)/\varepsilon_{\text{fr}}$	Various porous media
Neale and Nader [19]	$\tau = 2(3-\varepsilon_{\text{fr}})$	Isotropic spherical packing
Prager [20]	$\tau = (1+\varepsilon_{\text{fr}})/2$	Entropy analysis
Bridgemen [20]	$\tau = \varepsilon_{\text{fr}}^{0.5}$	–

error in prediction of heat transfer rate, the frost growth rate, and densification of the frost layer. If the heat transfer and growth rate, or densification rate are not very sensitive to the tortuosity factor, one may draw conclusions concerning how accurate the tortuosity equation must be.

3.1. Latent heat transfer rate by diffusion

Heat transfer occurs within the frost layer by conduction and water vapor diffusion. In this section, the magnitude of these two heat transfer modes are compared and the fraction of each heat transfer mode to the total heat transfer is discussed.

The heat flux by conduction may be approximated by the temperature gradient in the frost layer and the thermal conductivity of the frost layer:

$$q''_{\mathrm{fr,sen}} = \bar{k}_{\mathrm{fr}}(T_{\mathrm{fr}} - T_{\mathrm{w}})/x_{\mathrm{fs}}. \tag{27}$$

x_{fs} is the thickness of the frost layer. The latent heat flux by the water vapor diffusion may be approximated by the saturation humidity ratio gradient through the frost layer and the effective water vapor diffusion coefficient within the frost layer:

$$q''_{\mathrm{fr,lat}} = i_{\mathrm{sv}}\overline{D}_{\mathrm{eff}}\bar{\rho}_{\mathrm{a}}(W_{\mathrm{fs}} - W_{\mathrm{w}})/x_{\mathrm{fs}}. \tag{28}$$

The water vapor is assumed saturated in the frost layer for the purpose of the relative comparison and the saturated humidity ratio at the frost surface and at the cold plate are functions of temperature.

The latent heat transfer ratio (LHR) may be introduced to estimate the portion of the latent heat transfer rate through frost layer:

$$\begin{aligned}\mathrm{LHR} &= \frac{q''_{\mathrm{lat,fr}}}{q''_{\mathrm{lat,fr}} + q''_{\mathrm{sen,fr}}} \\ &= \frac{i_{\mathrm{sv}}\overline{D}_{\mathrm{eff}}\bar{\rho}_{\mathrm{a}}(W_{\mathrm{fs}} - W_{\mathrm{w}})}{i_{\mathrm{sv}}\overline{D}_{\mathrm{eff}}\bar{\rho}_{\mathrm{a}}(W_{\mathrm{fs}} - W_{\mathrm{w}}) + \bar{k}_{\mathrm{fr}}(T_{\mathrm{fs}} - T_{\mathrm{w}})}.\end{aligned} \tag{29}$$

To simplify Eq. (29), the function, $g(T_{\mathrm{fs}}, T_{\mathrm{w}})$ is introduced and defined as

$$g(T_{\mathrm{fs}}, T_{\mathrm{w}}) = (W_{\mathrm{fs}} - W_{\mathrm{w}})/(T_{\mathrm{fs}} - T_{\mathrm{w}}). \tag{30a}$$

The saturation humidity ratio is not linear with saturation temperature, and the function, $g(T_{\mathrm{fs}}, T_{\mathrm{w}})$ is not simple. However, the approximate value of the function $g(T_{\mathrm{fs}}, T_{\mathrm{w}})$ may be obtained at the average of T_{fs} and T_{w}:

$$g(T_{\mathrm{fs}}, T_{\mathrm{w}}) \approx \mathrm{d}W_{\mathrm{s}}/\mathrm{d}T_{\mathrm{s}}|_{T_{\mathrm{s}}=(T_{\mathrm{fs}}+T_{\mathrm{w}})/2}. \tag{30b}$$

The latent heat ratio can be simplified with the above function and the definition of the tortuosity factor (Eq. (26)):

$$\mathrm{LHR} = \frac{i_{\mathrm{sv}}\tau\varepsilon_{\mathrm{fr}}\overline{D}_{\mathrm{v}}\bar{\rho}_{\mathrm{a}}g(T_{\mathrm{fs}}, T_{\mathrm{w}})}{i_{\mathrm{sv}}\tau\varepsilon_{\mathrm{fr}}\overline{D}_{\mathrm{v}}\bar{\rho}_{\mathrm{a}}g(T_{\mathrm{fs}}, T_{\mathrm{w}}) + \bar{k}_{\mathrm{fr}}}. \tag{31}$$

In Eq. (31), factors other than $g(T_{\mathrm{fs}}, T_{\mathrm{w}})$ and thermal conductivity of the frost layer, may be treated as constant. The maximum error for the LHR, due to the uncertainty of tortuosity factor, occurs at the maximum value of $g(T_{\mathrm{fs}}, T_{\mathrm{w}})$. The maximum value of $g(T_{\mathrm{fs}}, T_{\mathrm{w}})$ occurs at 0 °C, which can be calculated using the water vapor saturation curve.

Fig. 5 shows the LHR vs. tortuosity factor for different values of porosity. For the analysis of limiting cases, the parallel and serial model for the thermal conductivity of the frost layer [4] were used, which give the maximum and minimum values of the frost layer thermal conductivity, respectively. Fig. 5a provides the results for the parallel model and Fig. 5b for the serial model for −1 °C. Fig. 5c and d shows the same comparisons for −20 °C. Calculations were performed for the LHR and total heat transfer rate for a ±14% variation of tortuosity factor about a mean value of 0.7. The 0.7 tortuosity factor was estimated for 300 kg/m^3 and was read from Fig. 5. The results are shown in Table 5. Table 5 shows that 14% uncertainty for the tortuosity factor affects the total heat transfer rate less than 3%. The reason the error is small is that the LHR is small compared to the total heat transfer rate.

The above analysis was conducted to investigate the effect of uncertainty in predicting the tortuosity factor. For the purpose, the extreme case that the value of $g(T_{\mathrm{fs}}, T_{\mathrm{w}})$ is taken near 0 °C (−1 °C) and the serial model for the thermal conductivity was considered. This value predicted the largest LHR shown in Table 5. The value of $g(T_{\mathrm{fs}}, T_{\mathrm{w}})$ decreases exponentially as temperature decreases. Hence, LHR and the error in predicting the total heat transfer rate exponentially decreases as the frost temperature decreases.

Consequently, an error in the range of 14% in the tortuosity factor will result in an insignificantly small error in the heat transfer rate in the frost layer.

3.2. Densification of the frost layer

The diffused water vapor changes phase within the frost layer, increasing the density of the frost layer. The thermal conductivity of the frost layer increases as the density of the frost layer increases.

The densification rate may be approximated as

$$\mathrm{d}\bar{\rho}_{\mathrm{fr}}/\mathrm{d}t = m''_{\mathrm{vd,fs}}. \tag{32}$$

The densification rate of the frost layer is dependent on the diffusion rate of water vapor at the frost surface. The average mass diffusion rate of the water vapor may be approximated as

$$m''_{\mathrm{vd,fs}} = \overline{D}_{\mathrm{eff}}\bar{\rho}_{\mathrm{a}}(W_{\mathrm{fs}} - W_{\mathrm{w}})/x_{\mathrm{fs}}. \tag{33}$$

This diffused water vapor sublimates within the frost layer and increases the frost density. As the frost layer grows more dense, the thermal conductivity of the frost

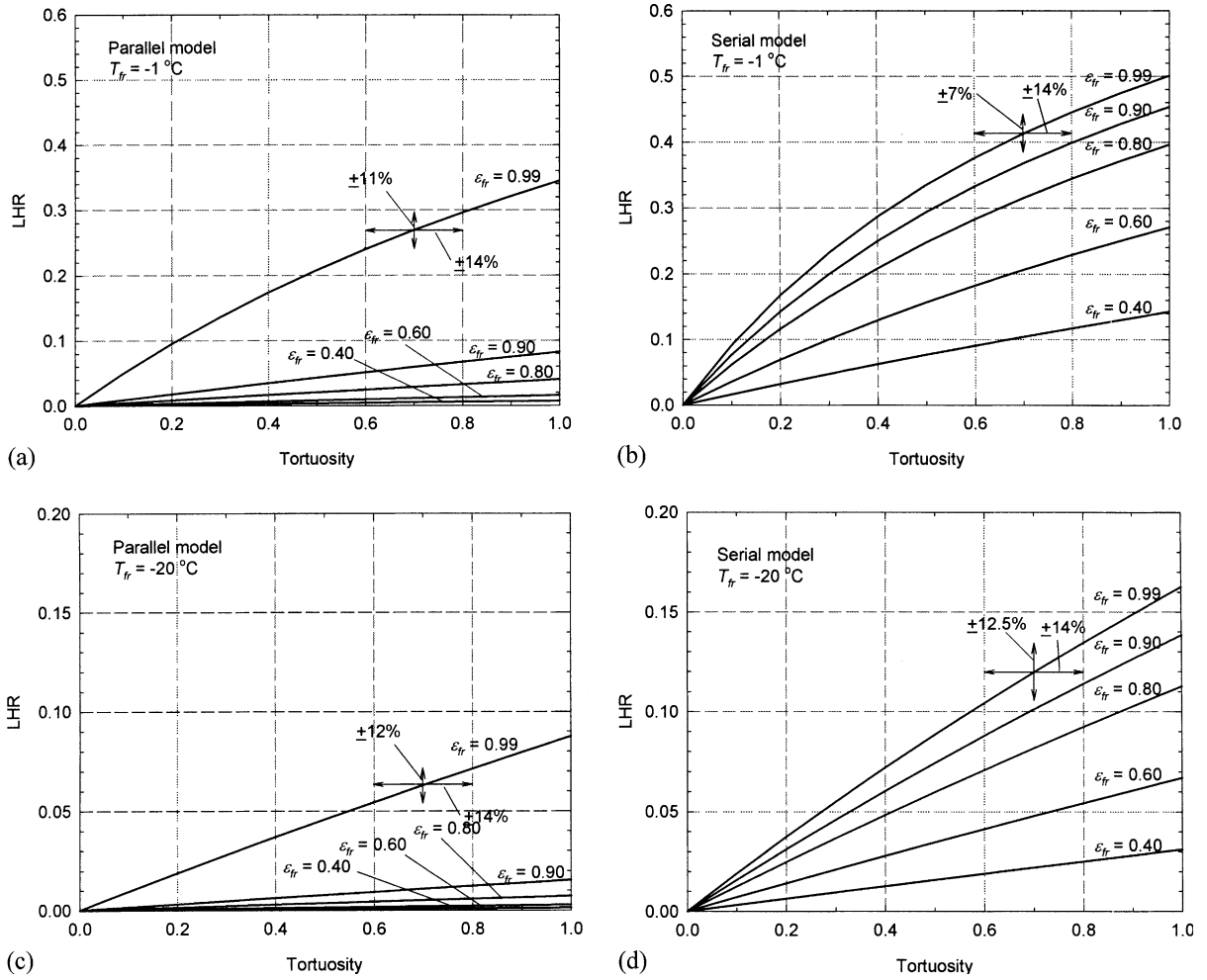

Fig. 5. Latent heat transfer ratio. Parallel model for thermal conductivity: (a) $T_{\mathrm{fr}} = -1$ °C, (c) $T_{\mathrm{fr}} = -20°$ C; serial model for thermal conductivity: (b) $T_{\mathrm{fr}} = -1$ °C, (d) $T_{\mathrm{fr}} = -20$ °C.

Table 5
Estimation of error for total heat transfer rate due to the tortuosity factor

Frost temperature (°C)	Thermal conductivity model	LHR (%)	Variation of LHR with 14% variation of tortuosity factor around 0.7 (%)	Error for total heat transfer rate (%)
−1	Parallel	27	±11	±3
	Serial	42	±7	±3
−20	Parallel	6.3	±12	±0.8
	Serial	12	±13	±1.6

layer increases. This rate of thermal conductivity change may be expressed as

$$\frac{\mathrm{d}\bar{k}_{\mathrm{fr}}}{\mathrm{d}t} = \frac{\partial\bar{\rho}_{\mathrm{fr}}}{\mathrm{d}t}\frac{\mathrm{d}\bar{k}_{\mathrm{fr}}}{\mathrm{d}\bar{\rho}_{\mathrm{fr}}}. \tag{34}$$

Eqs. (32)–(34) may be combined and the rate of thermal conductivity change is approximated as

$$\frac{\mathrm{d}\bar{k}_{\mathrm{fr}}}{\mathrm{d}t} = \overline{D}_{\mathrm{v,eff}}\bar{\rho}_{\mathrm{a}}\frac{W_{\mathrm{fs}} - W_{\mathrm{w}}}{x_{\mathrm{fs}}}\frac{\mathrm{d}\bar{k}_{\mathrm{fr}}}{\mathrm{d}\bar{\rho}_{\mathrm{fr}}}. \tag{35}$$

Using the tortuosity factor and the function, $g(T_{\mathrm{fs}}, T_{\mathrm{w}})$ defined by Eq. (30), Eq. (35) becomes

$$\frac{\mathrm{d}\bar{k}_{\mathrm{fr}}}{\mathrm{d}t} = \bar{\tau}\bar{\varepsilon}_{\mathrm{fr}}\overline{D}_{\mathrm{v}}\bar{\rho}_{\mathrm{a}}g(T_{\mathrm{fs}}, T_{\mathrm{w}})\frac{T_{\mathrm{fs}} - T_{\mathrm{w}}}{x_{\mathrm{fs}}}\frac{\mathrm{d}\bar{k}_{\mathrm{fr}}}{\mathrm{d}\bar{\rho}_{\mathrm{fr}}}. \tag{36}$$

To estimate the rate of thermal conductivity change for different values of tortuosity factor, the limiting thermal conductivity models (parallel model and serial models) are again used. The derivatives of thermal conductivity of the frost layer with respect to the density are for the parallel model:

$$\mathrm{d}k_{\mathrm{fr}}/\mathrm{d}\rho_{\mathrm{fr}} \approx \bar{k}_{\mathrm{ice}}/\bar{\rho}_{\mathrm{ice}} \tag{37a}$$

and for serial model:

$$\mathrm{d}\bar{k}_{\mathrm{fr}}/\mathrm{d}\bar{\rho}_{\mathrm{fr}} \approx (1/\bar{k}_{\mathrm{a}}\bar{\rho}_{\mathrm{ice}})(1/\bar{k}_{\mathrm{ice}} + \bar{\varepsilon}_{\mathrm{fr}}/\bar{k}_{\mathrm{a}})^{-2}. \tag{37b}$$

The temperature drop across the frost layer is also needed to estimate the ratio. In this estimation, the maximum value that may occur in a refrigeration evaporator is estimated. To estimate the maximum value, it is assumed that the dominant heat transfer resistance is in the frost layer. This means that heat transfer resistance for convection on the frost surface is negligible. The following values were used for the estimation analysis:

- air temperature: −20 °C,
- cold plate temperature: −25 °C,
- frost thickness: 0.5 mm.

Fig. 6 shows the $(\mathrm{d}\bar{k}_{\mathrm{fr}}/\mathrm{d}t)/\bar{k}_{\mathrm{fr}}$ ratio vs. tortuosity factor for both the parallel and serial thermal conductivity models with variation of the tortuosity factor. Fig. 6a shows the results for the parallel model and Fig. 6b is for the serial model. The maximum value of the ratio, $(\mathrm{d}\bar{k}_{\mathrm{fr}}/\mathrm{d}t)/\bar{k}_{\mathrm{fr}}$, occurs with the parallel model when the tortuosity factor and porosity of the frost layer are one. Even if the tortuosity factor and porosity of the frost layer are less than one, the value of one was used for the purpose of estimating the effect of the error in predicting the tortuosity factor on the densification rate, which affects the thermal conductivity of the frost layer. The maximum value is approximately 5×10^{-6} s^{-1}. Using this value, the thermal conductivity change rate can be calculated:

$$\mathrm{d}\bar{k}_{\mathrm{fr}}/\mathrm{d}t = 5\times10^{-6}\cdot\bar{k}_{\mathrm{fr}}\ [\mathrm{W/m\,K\,s}]. \tag{38}$$

The frost thermal conductivity changes less than 2% for 1 h. Hence, it may be concluded that the tortuosity factor or water vapor diffusion has an insignificant effect on the change of thermal conductivity with respect to time.

3.3. Frost growth rate

The effect of tortuosity factor on the frost growth rate is discussed in this section. This is done by estimating the ratio of the diffusion rate in the frost layer to the total transferred water vapor. This ratio is given by

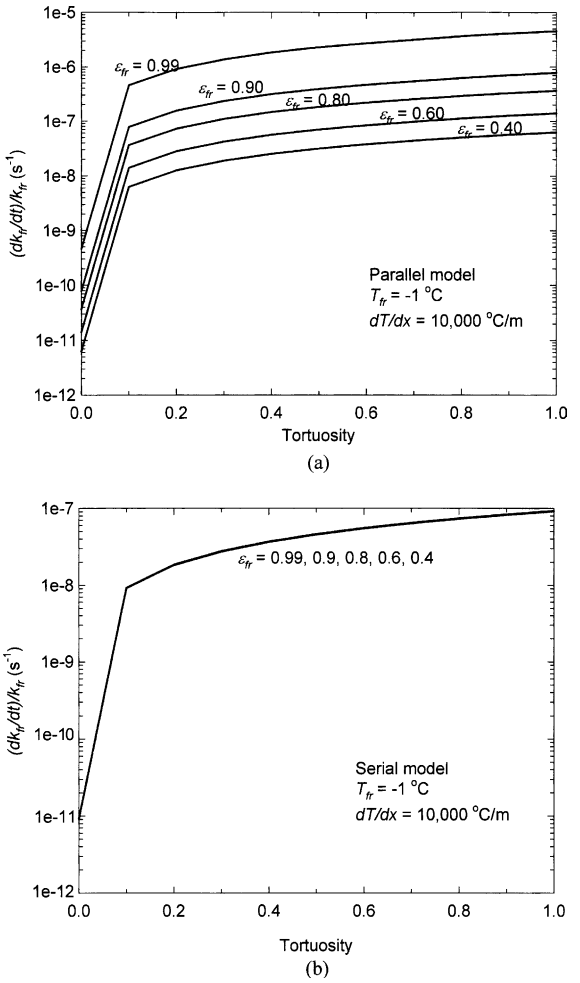

Fig. 6. Thermal conductivity change ratio: (a) parallel model for thermal conductivity; (b) serial model for thermal conductivity.

$$\begin{aligned}\text{Ratio} &= m''_{\mathrm{vd,fs}}/m''_{\mathrm{v}} \\ &\approx \tau\varepsilon_{\mathrm{fr}}D_{\mathrm{v}}[(W_{\mathrm{fs}}-W_{\mathrm{w}})/x_{\mathrm{fs}}]/K_{\mathrm{w}}(W_{\mathrm{a}}-W_{\mathrm{fs}}).\end{aligned} \tag{39}$$

The mass transfer coefficient, K_{w}, at the frost surface may be estimated using the heat and mass transfer analogy (Eq. (17)). The ratio defined in Eq. (39) is dependent on the environmental parameters. An order of magnitude analysis is useful to estimate the ratio in Eq. (39). Table 6 lists the absolute values of the variables in Eq. (39), and their orders of magnitude. The heat transfer coefficient, h, for the mass transfer coefficient was assumed to be 150 W/m^2 K, which is a reasonable value of air side heat transfer coefficient.

Using the order of magnitudes in Table 6, the order of the ratio in Eq. (39) is found to be 10^{-2}. This implies that the quantity of water vapor diffusing into the frost layer is less than 10% of the total water vapor transfer

Table 6
Base data for the order of magnitude analysis of Eq. (39)

Variables	Symbols	Values	Order of magnitude	Comments
Tortuosity	τ	0–1	1	Maximum value
Porosity	ε_{fr}	0–1	1	Maximum value
Diffusion coefficient (m^2/s)	D_v	1.45×10^{-5}–2.49×10^{-5}	10^{-5}	$T_a = -50$ to 20 °C
Air density (kg/m^3)	ρ_a	1.58–1.2	1	
Humidity ratio	W_a	0.0037	10^{-3}	0 °C
	W_{fs}	6.3×10^{-4}	10^{-4}	−20 °C
	W_w	2.4×10^{-5}	10^{-5}	−50 °C
Humidity ratio difference	$W_a - W_{fs}$	0.011	10^{-3}	
	$W_{fs} - W_w$	0.0038	10^{-4}	
Frost thickness (m)	x_{fs}	0.001	10^{-3}	
Specific heat of air (J/kg K)	c_p	1005	10^3	
Lewis number	Le	0.89	1	
Heat transfer coefficient (W/m^2 K)	h	150	–	
Mass transfer coefficient (m/s)	K_w	0.14	10^{-1}	

from the air stream to the frost layer. So, more than 90% of the mass transfer goes to increasing the frost thickness.

This order of magnitude analysis can be proved using the parallel model of frost structure. This model gives the maximum ratio of water vapor diffusion-to-the total mass transfer from the air stream to the frost layer. Using the parallel model, the tortuosity factor is one because the diffusion path is not tortuous. The water vapor diffusion rate may be expressed as

$$m''_{vd,fs} = D_v \varepsilon_{fr} \rho_a (W_{fs} - W_w)/x_{fs}. \quad (40)$$

The total mass transfer rate from the air stream to the frost layer is

$$m''_v = K_w (W_a - W_{fs}). \quad (41)$$

Using the values in Table 6 for calculating Eqs. (40) and (41), the ratio given in Eq. (39) becomes less than 7%. This means the order of magnitude analysis performed above is successful.

Therefore, it may be concluded that the quantity of the diffused water vapor is very small compared to that of deposited water vapor, and moderate error in predicting the tortuosity factor will have very small affect on the prediction of frost growth rate. As noted in the discussion of Fig. 4b, the tortuosity equations of Auracher [7], Neale and Nader [19], Prager [20], and Bridgemen [20] will all approximate that of frost for the expected porosity range of 0.6–0.9.

4. Conclusions

The analysis presented in this paper supports the following conclusions:

(1) When frost forms or grows on a cold surface, the water vapor is supersaturated at the frost surface. This is contrary to the assumption used by previous researchers, who assumed the water vapor is saturated at the frost surface.
(2) The mass transfer rate will be greatly overpredicted, if it is assumed that the air is saturated at the cold surface. Previously published frost models incorporate this assumption.
(3) The present model predicts the mass transfer rate within 0 to +25%.
(4) The tortuosity factor is relatively insensitive to the heat transfer through the frost layer, densification rate of the frost layer, and frost growth rate. The Prager correlation is recommended for analyzing the frost growth rate and densification.

References

[1] R.F. Barron, L.S. Han, Heat and mass transfer to a cryosurface in free convection, J. Heat Transfer 87 (4) (1965) 499–506.
[2] P.L.T. Brian, R.C. Reid, I. Brazinsky, Cryogenic frost properties, Cryog. Technol. 5 (1969) 205–212.
[3] P.L.T. Brian, R.C. Reid, Y.T. Shah, Frost deposition on cold surfaces, Ind. Eng. Chem. Fundam. 9 (3) (1970) 375–380.
[4] C.T. Sanders, The Influence of Frost Formation and Defrosting on the Performance of Air Coolers, Ph.D. thesis, Delft Technical University, 1974.
[5] B.W. Jones, J.D. Parker, Frost formation with varying environmental parameters, J. Heat Transfer 97 (1975) 255–259.
[6] S.M. Sami, T. Duong, Mass and heat transfer during frost growth, ASHRAE Trans. Part 1 95 (3218) (1989) 158–165.

[7] R. Le Gall, J.M. Grillot, Modeling of frost growth and densification, Int. J. Heat Mass Transfer 40 (13) (1997) 3177–3187.
[8] I. Tokura, H. Saito, K. Kishinami, Study on properties and growth rate of frost layers on cold surfaces, J. Heat Transfer 105 (1983) 895–901.
[9] K.S. Lee, W.S. Kim, T.H. Lee, A one-dimensional model for frost formation on a cold flat surface, Int. J. Heat Mass Transfer 40 (18) (1997) 4359–4365.
[10] Y.X. Tao, R.W. Besant, K.S. Rezkallah, A mathematical model for predicting the densification and growth of frost on a flat plate, Int. J. Heat Mass Transfer 36 (2) (1993) 353–363.
[11] H.W. Schneider, Equation of the growth rate of frost forming on cooled surface, Int. J. Heat Mass Transfer 21 (1978) 1019–1024.
[12] Y. Mao, R.W. Besant, H. Chen, Frost characteristics and heat transfer on a flat plate under freezer operating conditions, ASHRAE Trans. (4295) (1999) 231–251.
[13] B. Na, R.L. Webb, A fundamental understanding of factors affecting frost nucleation, Int. J. Heat Mass Transfer 46 (2003) 3797–3808.
[14] Y.A. Çengel, M.A. Boles, Thermodynamics, fourth ed., McGraw Hill, New York, 2002 (Chapter 16).
[15] P.W. Atkins, Physical Chemistry, sixth ed., Oxford University Press, Oxford, 1998 (Chapter 6).
[16] N.H. Fletcher, The Chemical Physics of Ice, Cambridge University Press, Cambridge, 1970.
[17] B. Na, Analysis of Frost Formation on an Evaporator, Ph.D. thesis, The Pennsylvania State University, 2003.
[18] B. Na, R.L. Webb, New model for frost growth rate, Int. J. Heat Mass Transfer, in press.
[19] G.H. Neale, W.K. Nader, Prediction of transport processes within porous media: diffusive flow processes within a homogeneous swarm of spherical particles, AIChE J. 19 (1) (1973) 112–119.
[20] R.E. Cunningham, R.J.J. Williams, Diffusion in Gases and Porous Media, Plenum Press, 1980.